An injectable, self-healing, 3D printable, double network co-enzymatically crosslinked hydrogel using marine poly- and oligo-saccharides for wound healing application

Applied Materials Today 29 (2022) 101581

Contents lists available at ScienceDirect

Applied Materials Today

journal homepage: www.elsevier.com/locate/apmt

An injectable, self-healing, 3D printable, double network co-enzymatically crosslinked hydrogel using marine poly- and oligo-saccharides for wound healing application

Hafez Jafari [a,*], Houman Alimoradi [b], Christine Delporte [c], Katrien V. Bernaerts [d], Reza Heidari [e], Daria Podstawczyk [f], Seyyed Vahid Niknezhad [g,*], Amin Shavandi [a,*]

[a] Université libre de Bruxelles (ULB), École polytechnique de Bruxelles, 3BIO-BioMatter, Avenue F.D. Roosevelt, 50 - CP 165/61, Brussels 1050 , Belgium
[b] School of Biomedical Sciences, University of Otago, Dunedin, New Zealand
[c] Laboratory of Pathophysiological and Nutritional Biochemistry, Medical School, Université Libre de Bruxelles, Route de Lennik, 808 – CP611, Brussels 1070, Belgium
[d] Maastricht University, Sustainable Polymer Synthesis Group, Aachen-Maastricht Institute for Biobased Materials (AMIBM), Brightlands Chemelot Campus, Urmonderbaan 22, 6167 RD Geleen, the Netherlands
[e] Pharmaceutical Sciences Research Center, Shiraz University of Medical Sciences, Shiraz, Iran
[f] Department of Process Engineering and Technology of Polymer and Carbon Materials, Faculty of Chemistry, Wroclaw University of Science and Technology, Norwida 4/6, Wroclaw 50–373 Poland
[g] Burn and Wound Healing Research Center, Shiraz University of Medical Sciences, Shiraz 71987-54361, Iran

ARTICLE INFO

Keywords:
Marine polysaccharides
Injectable hydrogels
Glucose oxidize
Enzyme-mediated crosslinking
Wound healing

ABSTRACT

In this study, we designed dual network hydrogels with antioxidant and antibacterial activities using marine poly- and oligosaccharides with skin wound healing potential. The synergy between dual enzymatic co-crosslinking based on glucose oxidize (GOx)/horseradish peroxidase (HRP) and electrostatic interaction between positively charged chitooligosaccharides (COS) and phenolated chitosan with negatively charged phenolated alginate formed a hydrogel. The Gel-COS hydrogels exhibited toughness, self-healing, moldability, injectability, and 3D printability. Investigation of the physicochemical properties of the hydrogels exhibited a swelling ratio (< 50%) and *in vitro* biodegradation after 9 days. Furthermore, the hydrogels exhibited antioxidant properties and antibacterial activity against *E. coli* and *S. aureus*. The hydrogels were not cytotoxic and enhanced the migration of 3D cell encapsulated 3T3-L1 fibroblasts, blood vessel formation, as well as *in vivo* wound healing in a rat model. The Gel-COS hydrogel can be considered a promising skin wound dressing material.

1. Introduction

The prevalence of acute skin wounds is growing fast because of the increasing frequency of type 2 diabetes, peripheral vascular disease, and metabolic syndrome, which hinder the wound healing process, and in some cases, cause amputation or mortality [1,2]. To address the limitations in chronic wound healing, a wide range of natural and synthetic compounds have been used as bioactive agents to accelerate the wound healing process by promoting proliferation and migration of fibroblast, increasing growth factors, and collagen production [3–5]. Hence, a bioactive compound with superior biological activities plays a prominent role in the efficacy of a wound dressing hydrogel [6]. Chitooligosaccharides (COS) are water-soluble depolymerized derivatives of chitosan with antibacterial, antioxidant, anti-inflammatory activity, as well as wound healing potential [7]. Besides, due to the short saccharide chains, COS is highly absorbed by the intestinal epithelia entering the blood flow and skin cell walls [8].

Hydrogels with the ability to provide a moist environment for the wound, allowing the penetration of oxygen, with the potential antibacterial properties and cell encapsulating or releasing of the bioactive agents, are considered ideal wound dressing materials [86]. In this regard, injectable multirole hydrogels which can encapsulate cells and bioactive agents, shape the wound and have antioxidant and antibacterial properties of special importance for skin wound healing[1,9]. The design of crosslinking method plays a significant role in the physicochemical and biological properties of the injectable hydrogel. Recently, enzymatic-triggered crosslinking reactions attracted a great deal of scientific consideration for hydrogel design in biomedical applications due

* Corresponding authors.
E-mail addresses: seyed.hafez.jafari@ulb.be (H. Jafari), vahidniknezhad@sums.ac.ir (S.V. Niknezhad), amin.shavandi@ulb.be (A. Shavandi).

https://doi.org/10.1016/j.apmt.2022.101581
Received 12 April 2022; Received in revised form 26 June 2022; Accepted 29 June 2022
Available online 15 July 2022

to their suitable cytocompatibility for cell encapsulation, adjustable mechanical properties, and mild reaction conditions in physiological conditions [10,11]. Horseradish peroxidase (HRP)-catalyzed hydrogel formation is a promising enzymatical crosslinking method to design injectable hydrogels because of its mild reaction and adjustable gelling time via tuning the crosslinking density and non-toxicity [12-14].

The enzymatic crosslinking process is not cytotoxic; however, using hydrogen peroxide (H_2O_2) for the enzyme activation can damage the tissue and inactivate the enzyme (HRP) at high concentrations [15]. To avoid using exogenous H_2O_2 in the reaction, glucose oxidase (GOx) has been used to catalyze the oxidation of glucose and the gradual release of H_2O_2 and D-glucono-δ-lactone (GDL), leading to a mild crosslinking process [16].

Various natural biopolymers such as polysaccharides and polypeptides have been used to form *in situ* injectable hydrogels for wound dressing due to their similarity to the natural extracellular matrix (ECM) [17,18]. As the second abundant marine polysaccharide, chitosan demonstrated wound healing potential due to its inherent antibacterial, antioxidant, biocompatibility, and hemostatic activity [19]. Chitosan-based injectable hydrogels using enzyme-mediated hydrogelation have been reported previously [20–22]. Due to its polycationic nature, chitosan can form polyelectrolyte complexes (PECs) with polyanionic polymers such as alginate and hyaluronic acid [23,24,87]. We previously showed that combining phenolated polyelectrolyte complex (PHEC) with HRP-catalyzed hydrogelation could improve the hydrogel's toughness, flexibility, and mechanical properties using phenolated chitosan and alginate due to the addition of dynamic non-covalent electrostatic interactions [25]. Besides, GDL, the byproduct of the GOx reaction, could play a role in the gelation process by inducing protonation of amine groups in the chitosan, which can lead to the improvement of electrostatic interactions between chitosan and alginate with different charge densities [26].

Owing to the presence of functional amine groups on the COS backbone, COS could increase the mechanical properties of the hydrogel by enhancing PHEC via the electrostatic interactions with the negatively charged alginate. In essence, COS provides the hydrogel with biological activity and increases the stability of the hydrogel.

Hence, in this study, a double network *in situ* injectable hydrogel using chitosan, alginate, and COS was designed by the synergy PHEC, and co-enzymatic-mediated crosslinking. The hydrogels were 3D printable, injectable, flexible, and moldable with suitable mechanical and self-healing properties favorable for irregular shape wounds as a minimally invasive approach. Furthermore, the hydrogels were not cytotoxic and demonstrated antibacterial, antioxidant, and angiogenesis activities, which induced the migration of fibroblast cells. Hence, the wound healing process in a full-thickness skin defect model was accelerated due to the high biological activities of hydrogel, resulting in inflammation inhibition, angiogenesis, and re-epithelization enhancement. This 3D printable hydrogel has the potential to be used for skin wound healing and as a bioink for different tissue engineering applications.

2. Materials and methods

2.1. Materials and reagents

Chitosan with a deacetylation (DD) degree ≥75%, sodium alginate, 1-ethyl-3-(3dimethylaminopropyl)carbodiimide (EDC) (98 %), N-hydroxysuccinimide (NHS) (98%), horseradish peroxidase (HRP), glucose oxidase (Gox), Congo Red (Dye content ≥35%), lysozyme (BioUltra, lyophilized powder, ≥98%, ≥40,000 units/mg protein), Hoechst (H33342) and ethidium homodimer I (E1903), D-(+)-Glucose, and hydrogen peroxide (H_2O_2) (30%) were purchased from Sigma Aldrich (St. Louis, MO, USA). Deuterium oxide (D_2O) and trifluoroacetic acid-*d* (CF_3COOD) were purchased from Eurisotop (Saint-Aubin, France). 3-(4-Hydroxyphenyl) propionic acid (> 99%) and tyramine hydrochloride (>98%) were obtained from Carbosynth (Compton, United Kingdom). The DPPH[1] Antioxidant Assay Kit was purchased from Dojindo Laboratories (Kumamoto, Japan). Ethanol absolute (99% +) and Cell Tracker Blue CMAC (7-amino-4-Chloromethylcoumarin), dialysis tube (3.5 MWCO, 35 mm), and PBS (phosphate-buffered saline) tablets were purchased from Thermo Fisher Scientific (Waltham, MA, USA).

2.2. Chitooligosaccharides (COS), Chitosan-phenol (Ch-Ph), and Alginate-Tyramine (Alg-Ty) preparation

COS with a molecular weight of 1–3 kDa was prepared and characterized by microwave-assisted oxidative degradation of chitosan as previously described [27]. Chitosan-Phenol (Ch-Ph) and Alg-Ty were prepared by conjugating 3-(4-hydroxyphenyl) propionic acid (HPA) and tyramine hydrochloride, respectively, via EDC/NHS chemistry, according to our previous report [25]. The conjugation of phenolic groups into the chitosan and alginate backbones was monitored using ^{1}H NMR and Ultraviolet-visible spectroscopy. ^{1}H NMR analysis was performed at 25 °C using a JEOL JNM-ECZ600R/S3 spectrometer operating at 14.1 T (600.17 MHz) equipped with a double 35 resonance ROYALTM probe. Unmodified chitosan was dissolved in 2 % V/V CF3COOD/D2O. Other samples (alginate, conjugated chitosan, and alginate) were dissolved in D_2O.

Ultraviolet-visible spectra were assessed using a UV/Vis PerkinElmer spectrophotometer, and the phenol content was calculated by measuring the absorbance of conjugated samples at 275 nm by comparison with a standard curve of 3-(4-hydroxyphenyl) propionic acid (HPA), and tyramine hydrochloride obtained by dissolving different concentrations (25–1000 μM) of HPA and Ty in distilled water[28].

2.3. Hydrogels preparation

Hydrogels were prepared in 1 mL vials at 37 °C based on the method described by [29] with some modifications. Ch-Ph (1.5 wt%) and Alg-Ty (1.5 wt%) aqueous solutions were dissolved in DIW and mixed with a volume ratio of 1:1 to form a PHEC by dropwise addition of the Alg-Ty solution to the Ch-Ph. The PHEC was stirred for two h to obtain a homogenized viscous PHEC. COS (1 mg/mL) was incorporated into the PHEC and was vortexed for 30 min. The hydrogels were formed by co-enzyme mediated crosslinking using HRP and Gox. Two PHEC suspension (100 μL) were prepared in a microtube vial, one containing HRP and glucose, and the other one included Gox. Then, the two solutions were mixed gently, and the gelation time was determined by the tube inversion method[29]. The final concentration of HRP, Gox, glucose, and COS were (1, 5, and 10 U/mL), 10 U/mL, 5.5 mM, and 1 mg/mL respectively. The Hydrogels were named Gel-COS 0 (without COS) and Gel-COS 1 (containing 1 mg/mL COS).

2.4. Physicochemical Characterization

2.4.1. Swelling ratio and in vitro degradation

The equilibrium swelling ratio of the hydrogels was investigated using the method previously described [30]. The hydrogels were soaked in the PBS solution ((pH 7.4, 0.01 M)) at 37 °C for 36 h to obtain the equilibrium swelling. After removing swollen hydrogels, filter papers were used to remove their excess water. The equilibrium swelling ratio was calculated by the following equation:

$$\text{Equilibrium swelling ratio (ESR)} = \left(\frac{W_1 - W_0}{W_0}\right) \times 100 \quad (1)$$

Where W_0 and W_1 are the weight of hydrogels before and after swelling, respectively.

[1] 2,2-diphenyl-1-picrylhydrazyl

In vitro enzymatic degradation of the hydrogels was investigated by the gravimetric method [31]. Hydrogels (300 μl) were prepared and accurately weighted (W_0), then the hydrogels were immersed at 37 °C in the PBS solution containing lysozyme (1 mg/mL). At different time intervals, the hydrogels were removed, excess superficial media was removed, and weighed (W1). After each time interval, new media were added to samples. The *in vitro* degradation was evaluated by determining the remaining mass of the samples using (W_1/ W_0) ×100 %.

2.4.2. Morphology of the hydrogels

The microstructure of the Gel-COS hydrogels was examined under a scanning electron microscope (SEM) (Hitachi SU-70). Before the experiment, the hydrogels were freeze-dried, cross-sectioned, and coated with gold.

2.4.3. Zeta potential

The zeta potential of the hydrogel precursor components (Ch-Ph, and Alg-Ty) was measured using a Malvern Zetasizer Ultra (Malvern Instruments Ltd., Malvern, UK). The experiment was conducted at 25 °C with an angle detection of 90° [32].

2.5. Rheological and self-healing properties of Gel-COS hydrogels

The rheological measurement of Gel-COS hydrogels was performed using a rheometer (Anton Paar MCR 302, Austria) equipped with a plate-plate geometry (25 mm) at 37 °C. 300 μL of hydrogels were *in situ* formed on the rheometer plate. First, the viscosity and shear thinning behavior of gel precursors were determined over a range of shear rates (0.1–1000 1/s). Then, the gelation kinetic was monitored using a time sweep test at the constant frequency (1 Hz) and strain (0.1%). To determine the linear viscoelastic region (LVR), an amplitude sweep (1 to 1000%) was performed at the constant frequency of 1 Hz [30]. The frequency sweep test was performed at a frequency range from 0.1 to 50 Hz and a constant strain (0.1%) [33].

The self-healing properties of Gel-COS hydrogels were evaluated by macroscopic observations and rheological investigation [34]. First, two Gel-COS hydrogels (400 μL) were formed, and one of them was stained with Congo red, and the gels were contacted together to a circular shape. After 5 min, the healed hydrogel was stretched to show the rapid self-healing performance. For the rheological analysis, G' and G" values of the hydrogels were determined via a step-strain test, performing four cycles of low strain (1%) and high strain (300%).

2.6. Antioxidant activity

The antioxidant activity of the hydrogels was investigated using the DPPH radical scavenging assay [29]. Briefly, 300μL of distilled water (control group) or the hydrogels were disposed of in a 48-well plate. Then, 1 mL of ethanol containing DDPH (100μL, 0.5 mM) was added followed by incubation for 30 min in the dark. The absorbance of hydrogels and control were measured using a microplate reader (Epoch microplate, BioTek Instruments, Inc., Winooski, VT, USA). The antioxidant activity was determined by the following equation:

$$\text{Radical scavenging activity } (\%) = [1 - (As / Ac)] \times 100 \quad (2)$$

Where A_s and A_C are the absorbances of samples, and the control (distilled water), respectively.

2.7. Antibacterial activity

The antibacterial activity of the Gel-COS hydrogels was investigated against Gram-negative bacteria (*Escherichia coli* ATCC 27,195) and gram-positive bacteria (*Staphylococcus aureus* ATCC 25,923) using growth inhibition test [35] and a colony counting assay [36]. Briefly, hydrogels (100 μL) were prepared in a 48 wells plate, and incubated with 1 mL of bacterial suspension (10^5 CFU/mL) in Muller–Hinton (M–H) for 24 h at 37 °C. Then, the absorbance of bacterial suspension treated in the presence and absence of Gel-COS hydrogels was determined at 600 nm using a microplate reader. For the colony counting assay, 100 μL of bacterial suspension (10^5 CFU/mL) incubated with the hydrogels (24 h at 37 °C) was spread uniformly on a Muller–Hinton (M–H) agar plate using a sterile swap and incubated at 37 °C. After 24 h, the plates were photographed to investigate the antibacterial activity of the hydrogels. All experiments were carried out in triplicate.

2.8. In vitro cytotoxicity and cell proliferation

Fibroblasts 3T3-L1, provided by Dr. I. Pirson were grown in DMEM (Dulbecco's Modified Eagle Medium) supplemented with 10% fetal calf serum (FCS), penicillin (200 U/mL), and streptomycin (200 U/mL) under a humidified atmosphere containing 5% CO_2 at 37 °C.

The toxicity of Gel-COS hydrogels was evaluated using 3T3-L1 mouse fibroblast cells by a CellTiter 96® AQueous One Solution Cell Proliferation Assay (MTS, Promega) and a live/dead assay. Briefly, gel precursor solutions were sterilized via sterile 0.22 μm syringe filters (Millipore Corporation, USA) prior to gel formation. 100 μL of the gel precursor ([Ch-Ph, Alg-Ty]= 1.5 wt%, [GOx]= 10 U/mL, [HRP]= 10 U/mL, [Glucose] = 5.5 mM) with COS (0, and 1 mg/mL) were prepared in a 96-well plates followed by incubating at 37 °C for 30 min to form a stable gel. 3T3-L1 cells (5×10^4 cells/well) were seeded on the hydrogels and incubated for three days. The cytotoxicity of the hydrogels was evaluated on days one and three using MTS assay [37]. Briefly, 20 μL of MTS solution was added to the wells followed by incubation for four h. The cell viability was determined by measuring the absorbance of the samples and the control at 490 nm using a plate reader. The mean absorbance of the control was considered as 100 % viability, and the samples were evaluated compared to the control.

Moreover, the cell viability and proliferation of 3T3-L1 cells encapsulated into the hydrogel were investigated by a live/dead assay. For 3D cell encapsulation, 3T3-L1 cell suspensions were mixed with the PHEC containing HRP (10 U/mL) and GOx (10 U/mL) to obtain a homogenous suspension with a final cell density of 5×10^5 cells/mL. Then, 50 μL of cell encapsulated PHEC in the absence and presence of COS (1 mg/mL) was mixed with a 50 μL PHEC containing glucose (5.5 mM) in a Millicell EZ SLIDE 8-well glass (Merck, Kenilworth, NJ, USA). . Then, 1 mL culture media was added to the wells, and the hydrogels were incubated at 37 °C for three days. The cell viability and distribution was investigated using Hoechst/ ethidium homodimer I (EH1) staining [38]. Briefly, 10 μM Hoechst and 2 μM EH1 were used to stain the cells for 20 min followed by washing with PBS (two times). The cells were fixed using paraformaldehyde (4%) for 20 min, and nuclei distribution were assessed by a fluorescent microscope (Zoe fluorescent cell imager, Biorad, Hercules, CA).

2.9. In vitro wound healing assay

The effect of Gel-COS hydrogels on the 3T3-L1 cells migration was investigated using an Ibidi culture insert 2 well (Ibidi, Gräfelfing, Germany). Briefly, the cells were seeded at a cell density of 230,000 cells/well in a culture medium containing 10% FCS and incubated for 24 h to reach cell confluency of 80 %. After 24 h, the cultured media was replaced with a culture medium containing 0.1% FCS to prevent cell proliferation. The hydrogels (600 μl) were formed and washed with PBS, followed by incubating in a 4 mL culture medium containing 0.1% FCS for 24 h to obtain the extracted hydrogel solution. Before treating the cells with the extracted hydrogel solution or culture medium (control), the cells were stained with 10 μM of cell blue tracker (Thermofisher, Waltham, MA, USA) according to the manufacturer's protocol. Finally, the culture inserts were removed, and the cells were treated with the extracted hydrogel solutions and control (cell culture medium containing 0.1% FCS) for 48 h. At 0, 24, and 48 h after removing the inserts, digital photographs were taken and the width of the remaining cell-free

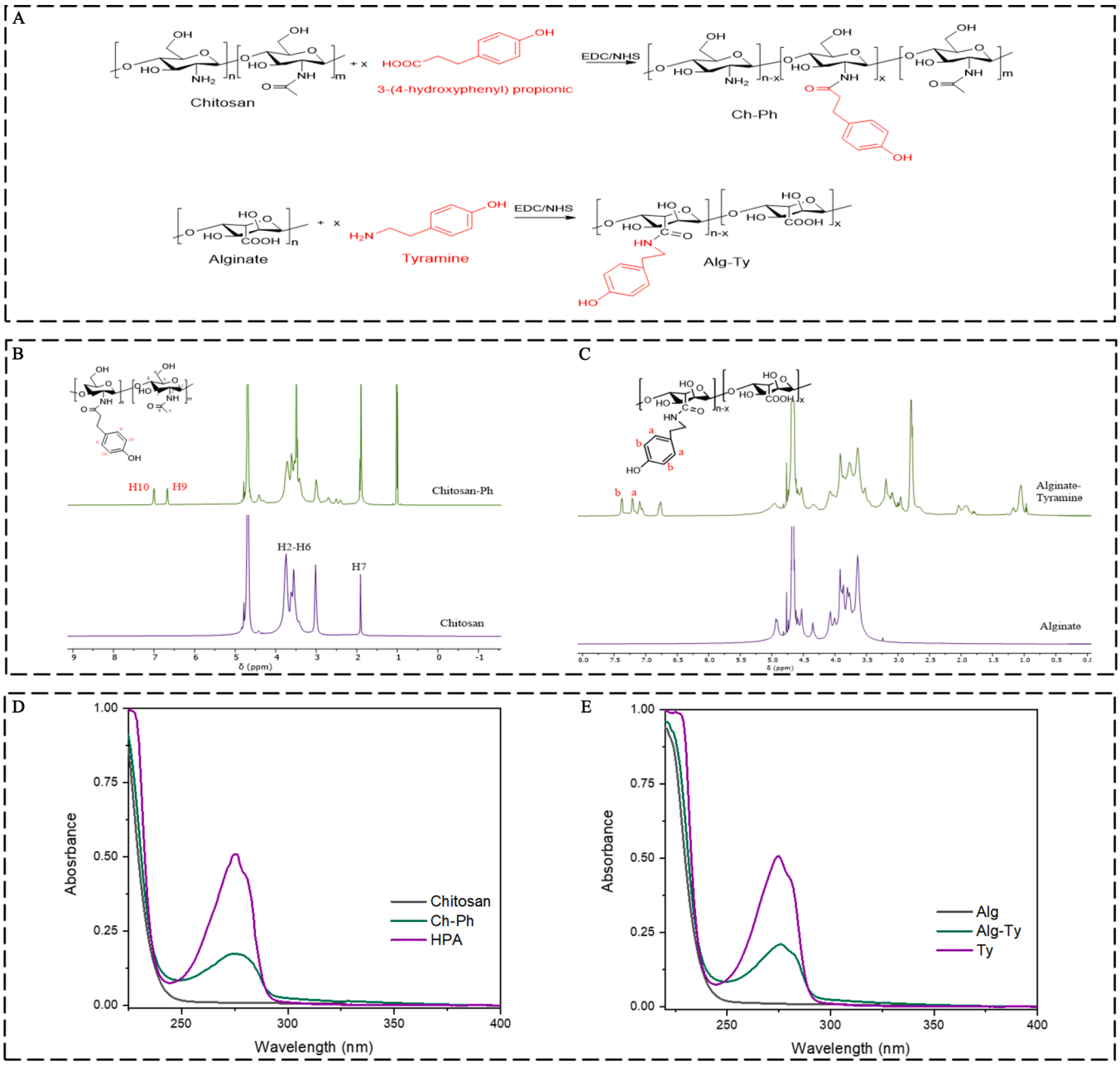

Fig. 1. (A) Synthetic scheme of the chitosan3-(4-hydroxyphenyl) propionic acid (Ch-Ph) and alginate-tyramine (Alg-Ty) conjugates; (B) ^{1}H NMR spectra of the Ch-Ph and unmodified chitosan; (C) ^{1}H NMR spectra of the Alg-Ty and unmodified alginate; (D) UV–vis spectra of Ch-Ph, unmodified chitosan, and 3-(4-hydroxyphenyl) propionic acid (HPA); (E) UV–vis spectra of Alg-Ty, unmodified alginate, and tyramine.

gap was measured using Image J software (1.8.0, https://imagej.nih.gov/ij/). All experiments were carried out in triplicates.

2.10. Chorioallantoic membrane (CAM) assay

CAM assay was carried out to investigate the biocompatibility and effects of the Gel-COS hydrogels on vascular sprouting and angiogenesis according to a previously described method [39]. Fertilized eggs were purchased from Belgabroed NV (Merksplas, Belgium). To rub off any dirt or feces and clean the eggs, they were gently washed with 37 °C water for a few minutes and dried using clean tissues. The eggs werethen incubated at 37 °C and 60% humidity. On day 4 of incubation, the eggs were wiped with 70% EtOH, the shells were cracked, and embryos were transferred to the culture petri dish. 200 μL of the hydrogels were placed on the yolk near one major blood vessel, and then the eggs were incubated for another 24 h. Digital pictures at a fixed distance were taken at 0 and 24 h after placing the hydrogels using a Nikon digital Camera (D5600 DSLR, Tokyo, Japan). For image analysis, initially, the vessels' path was manually drawn using Adobe Illustrator (CS6), then the background was removed entirely, and the resulting images were quantitatively analyzed by Angiogenesis Analyzer in Fiji ImageJ [40]. Each analysis is normalized based on the vessel formation of a similar section of the same embryo, and the results are expressed as fold changes in total segment length and fold changes in the number of segments.

2.11. Animal Care and Surgical Procedure

Male Sprague Dawley rats (n=36; 250–300 g weight) were obtained from the Laboratory of Animals Breeding Center (Shiraz University of Medical Sciences, Shiraz, Iran). Animals were housed in plastic cages

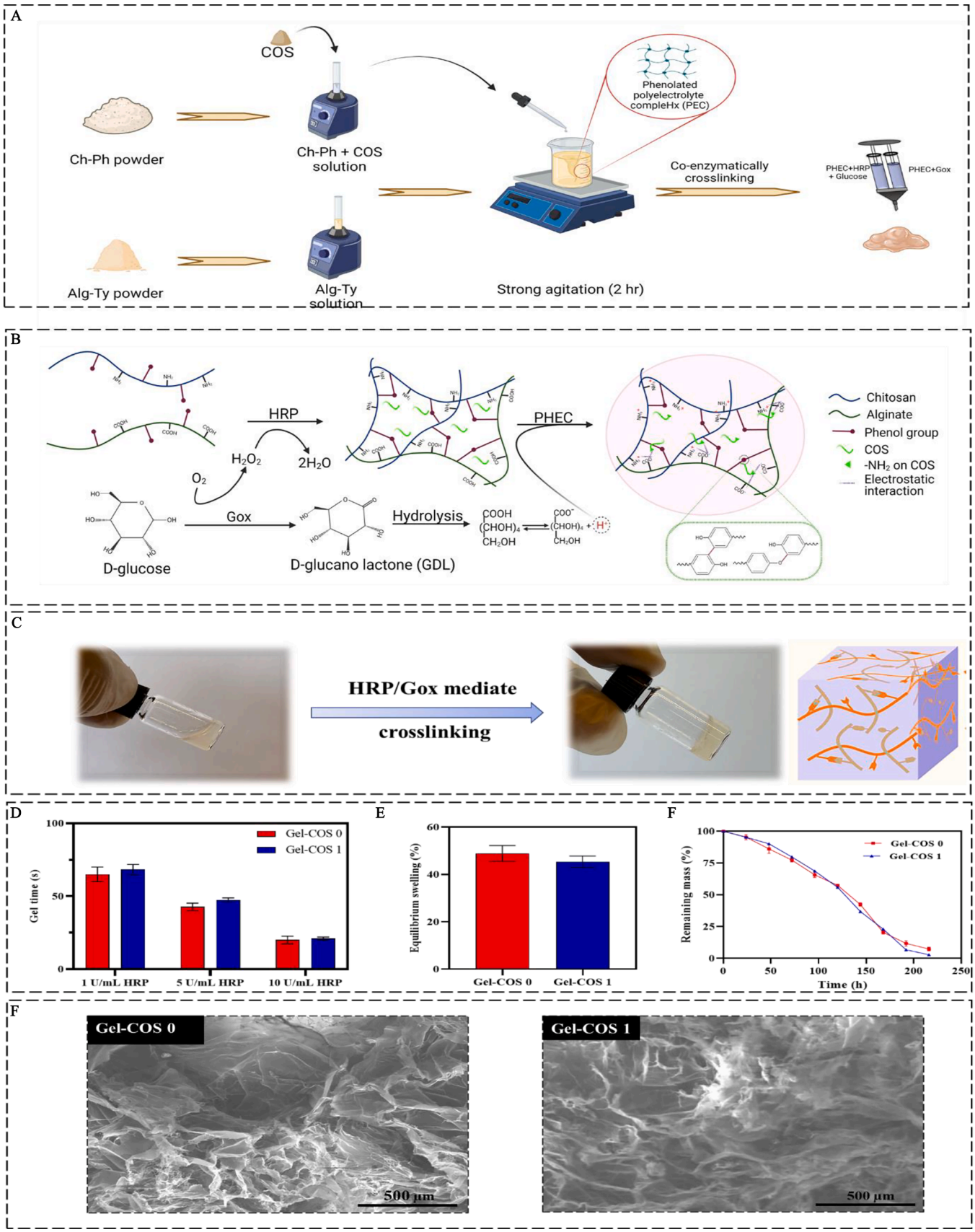

(caption on next page)

Fig. 2. (A) Schematic route of the Gel-COS preparation process starting with the dissolution and mixing of Ch-Ph, COS, and Alg-Ty, and formation of viscous phenolated polyelectrolyte complex (PHEC) via electrostatic interactions, and subsequent hydrogel formation by co-enzymatically crosslinking using horseradish peroxidase (HRP) and glucose oxidase (Gox); (B) Schematic illustration of possible interactions in Gel-COS hydrogel preparation by the synergy of co-enzymatically mediated crosslinking (HRP and Gox) triggered by glucose and phenolated polyelectrolyte complex (PHEC) between positively charged chitosan and COS with negatively charged alginate. GOx reacts with the glucose and gradually releases H_2O_2 leading to the HRP activation and the crosslinking initiation; besides, the GDL as a byproduct of the Gox reaction can release protons, enhancing the electrostatic interaction; (C) Photograph of PEC solution before and after gelation via co-enzymatically mediated crosslinking using HRP and Gox; (d) Gelation time of the Gel-COS 0 and Gel-COS 1; (E) Equilibrium swelling ratio of hydrogels after 36 h at 37 °C; (F) *In vitro* enzymatic degradation of the Gel-COS hydrogels in lysozyme solution (1 mg/mL) at 37 °C; (G) Scanning electron microscopy (SEM) microstructure images of Gel-COS hydrogels.

over woodchip bedding in a standard environment (23 ± 1 °C, 12:12 light: dark cycles, 40% relative humidity). During experiments, rats were allowed free access to tap water and a regular standard rodents chow diet (Behparvar®, Tehran, Iran). All experiments in this study were conducted according to appropriate ethical guidelines, approved by the ethics committee at Shiraz University of Medical Sciences (Shiraz, Iran) (Approval ID: IR.SUMS.REC.1401.007).

Briefly, animals were first anesthetized with an intraperitoneal administration of ketamine 10% (100 mg/kg) and xylazine 2% (5 mg/kg). Full-thickness skin circular wounds with 12 mm diameter were created on the rat skin. Six animals per time point (7 and 14 days) per condition were used for the experimental control group (PBS) and treated with, Gel-COS 0 and Gel-COS 1 hydrogels.

2.12. In Vivo Wound Healing Test

The wound healing process was monitored by taking photos of the wounds on days 1, 4, 7, 11 and 14 after treatment. The wound healing ratio was calculated as follows: Wound healing ratio = (A0 – A)/(A0) × 100%, where A0 and A are the area of the initial wound and current wound, respectively. At the predetermined time points (7 and 14 days), rats were euthanized, and skin tissue for each animal was fixed overnight in 10% formalin buffer (0.4% w/v NaH_2PO_4, 0.64% w/v Na_2HPO_4, and 10% v/v formaldehyde in double-distilled water). Then, the fixed tissues were paraffin-embedded and cut into 5-μm sections, which were dewaxed using xylene followed by dehydration using gradient alcohol. The slides were stained using hematoxylin-eosin (H&E) and Masson's trichrome staining according to established protocols. Blind reading of histological analysis was conducted to assess the wound healing. A light microscope (Olympus CX21®, Japan) were used for imaging and parameters including the Granulation tissue thickness and Scar width (mm) were quantitatively compared using ImageJ for the different experimental groups.

2.13. Statistical analysis

All experiments were carried out in triplicates, and the results were expressed as means ± standard deviations. Statistical analyses were conducted using GraphPad Prism 8 (GraphPad Software Inc.) using one-way ANOVA followed by Tukey's post-hoc analysis. *P*-values < 0.05 were considered statistically significant and indicated by *.

3. Results and discussion

3.1. Synthesis of Ch-Ph and Alg-Ty conjugates

The synthetic process of Ch-Ph and Alg-Ty conjugates was demonstrated in Fig. 1a. Ch-Ph and Alg-Ty were conjugated using a carbodiimide/active ester-mediated coupling reaction in the presence of EDC and NHS (Fig. 1A) [41,42]. ^{1}H NMR spectra (Fig. 1B) exhibited new signals around 6.6–7.2 ppm for Ch-Ph attributed to the phenol groups' aromatic ring protons, indicating the successful conjugation of propionic acid into the chitosan backbone [43]. Furthermore, the UV spectra (Fig. 2C) displayed a new peak at 275 nm for Ch-Ph, which aligns with the ^{1}H NMR results confirming the successful conjugation of propionic acid on the chitosan backbone [88].

Similar to chitosan, alginate was modified with tyramine using EDC/NHS (Fig. 1A). ^{1}H NMR (Fig. 1C) and UV spectra (Fig. 2E) confirmed tyramine's conjugation into the alginate backbone. Two new signals at around 7.2–7.4 in ^{1}H NMR spectra of Alg-Ty and a new peak at 275 nm in the UV spectra of Alg-Ty indicate that alginate was successfully modified by tyramine groups [44]. Moreover, the phenol content of both Ch-Ph and Alg-Ty was calculated based on UV spectra. Ch-Ph and Alg-Ty exhibited a phenol content of 356 and 280 μmole per gram of polymers, respectively.

3.2. Hydrogel formation

Although the HRP-mediated crosslinking strategy is a biocompatible method for hydrogel preparation, H_2O_2 as an oxidizing agent to activate the HRP is rising concerns for direct cell encapsulation due to the adverse effect of H_2O_2 on cell viability[15]. Glucose oxidase (GOx) can gradually generate H_2O_2 by consuming O_2 and glucose. Hence, the gradual release of H_2O_2 by GOx activates the HRP during the gel formation process resulting in a hydrogel with more cytocompatibility compared to the direct use of H_2O_2. We previously showed that the phenolated chitosan and alginate could form a PHEC due to their different charge densities [25]. A viscous PHEC was therefore obtained after mixing the Ch-Ph and Alg-Ty and COS via dropwise addition of the Alg-Ty solution to Ch-Ph solution containing COS followed by strong agitation to homogenize the formed PHEC . Moreover, the zeta potential of Ch-Ph, and Alg-Ty was measured; the Ch-Ph exhibited a zeta potential of 7.3 ± 0.8 mv, while the zeta potential of Alg-Ty was −23.6 ± 3.9 mv. The results confirmed the presence of positive charge of Ch-Ph, and negative surface charge of Alg-Ty solution.

The PHEC formation was induced by the electrostatic interaction between free amino groups of chitosan and COS with carboxyl groups of alginate prior tothe co-enzymatically crosslinking of phenol moieties on the chitosan and alginate backbones (Fig 2A).

Subsequently, the PHEC was used to form a hydrogel by co-enzymatically mediated crosslinking (HRP and GOx) initiated by glucose. Unlike the endogenous use of H_2O_2, in GOx/glucose cascade reaction, H_2O_2 can be provided via the catalysis of GOx in a mild way leading to a mild enzymatic crosslinking of the phenol functionalized polymers [15,45]. Additionally, GDL which is the byproduct of the glucose oxidation reaction can gradually donates protons due to its hydrolyzation, leading to an increase in the protonation degree of chitosan and COS, which results in the improvement in the electrostatic interactions with negatively charged alginate (Fig. 2B) [24,46].

The gelation time of Gel-COS hydrogels and the effect of HRP concentration were investigated via the vial inversion method (Fig. 2C,D). The effect of different concentrations of HRP on the gelation time of Gel-COS hydrogels was investigated, and the gelation of Gel-COS 0 and Gel-COS 1 were 66.3 ± 3.3 and 68.3 ± 2.2 s respectively when the HRP concentration was 1 U/mL. Increasing the HRP concentration from 1 to 10 U/mL accelerated the gelation time of Gel-COS 0 and Gel-COS 1 hydrogels to 19.1 ± 2.9 and 20.4 ± 2.1 s, respectively, indicating the effect of the HRP concentration on the gelation time. Moreover, the results showed that the COS incorporation did not affect the gelation time.

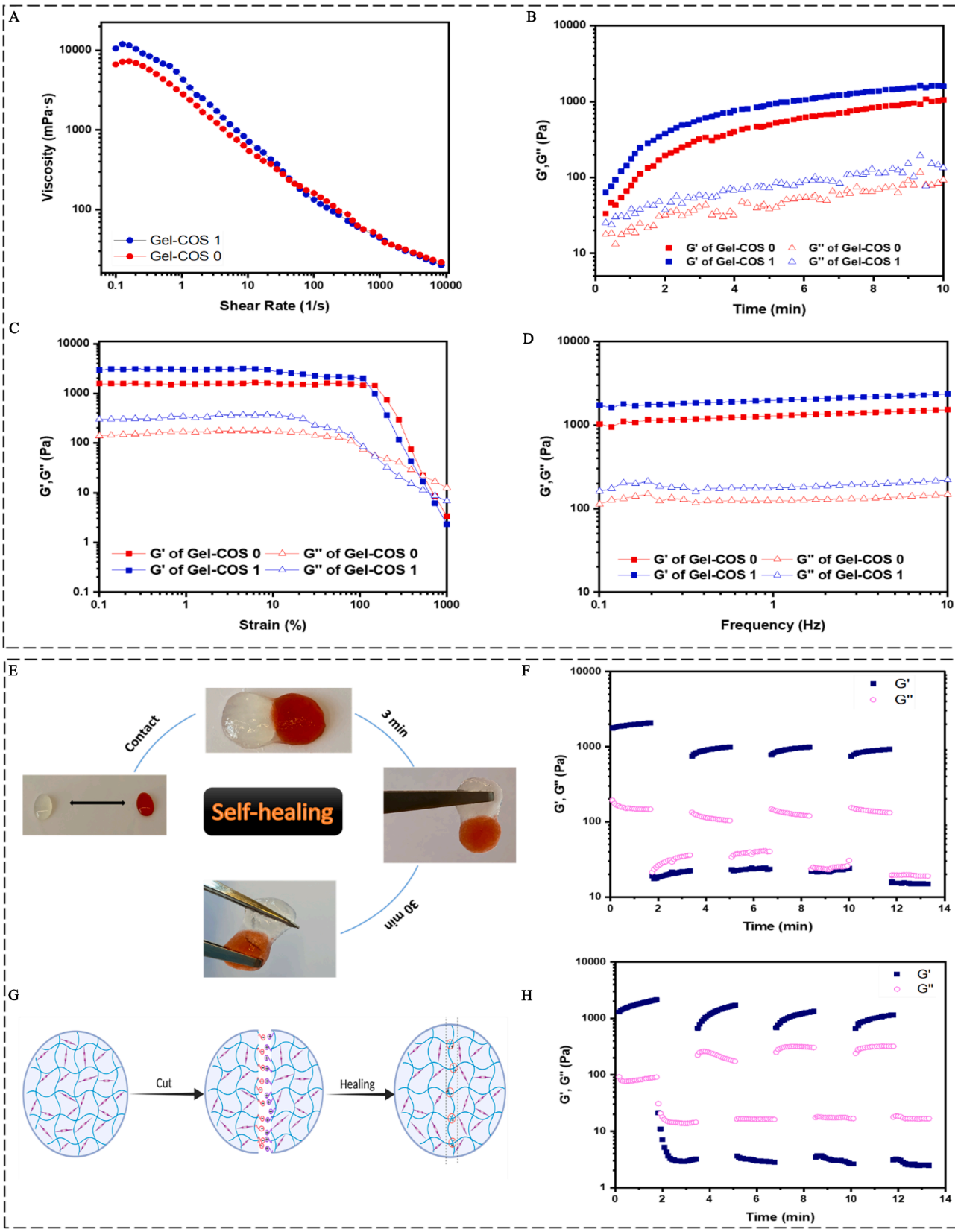

Fig. 3. Viscoelastic features of the Gel-COS hydrogels. (A) shear-rate dependent variations of dynamic viscosity of Gel-COS gel precursor (37 °C); (B) Gelation kinetics of Gel-COS hydrogels determined by a time sweep test at a constant strain (0.1 %) and frequency (1 Hz) at 37 °C; (C) The amplitude sweep test of Gel-COS hydrogels at a constant frequency of 1 Hz at 37 °C; (D) The frequency sweep test of Gel-COS hydrogels at a constant strain of 1 % at 37 °C; (E) Macroscopical photographs of cut-contacted Gel-COS hydrogels for the self-healing behavior observation; (F) Rheological assessment of Gel-COS 0 hydrogel self-healing capability (strain = 1% / 300% /1%...); (G) Schematic illustration for self-healing mechanism of Gel-COS hydrogel; (H) Rheological assessment of Gel-COS 1 hydrogel self-healing capability (strain = 1% / 300% /1%...).

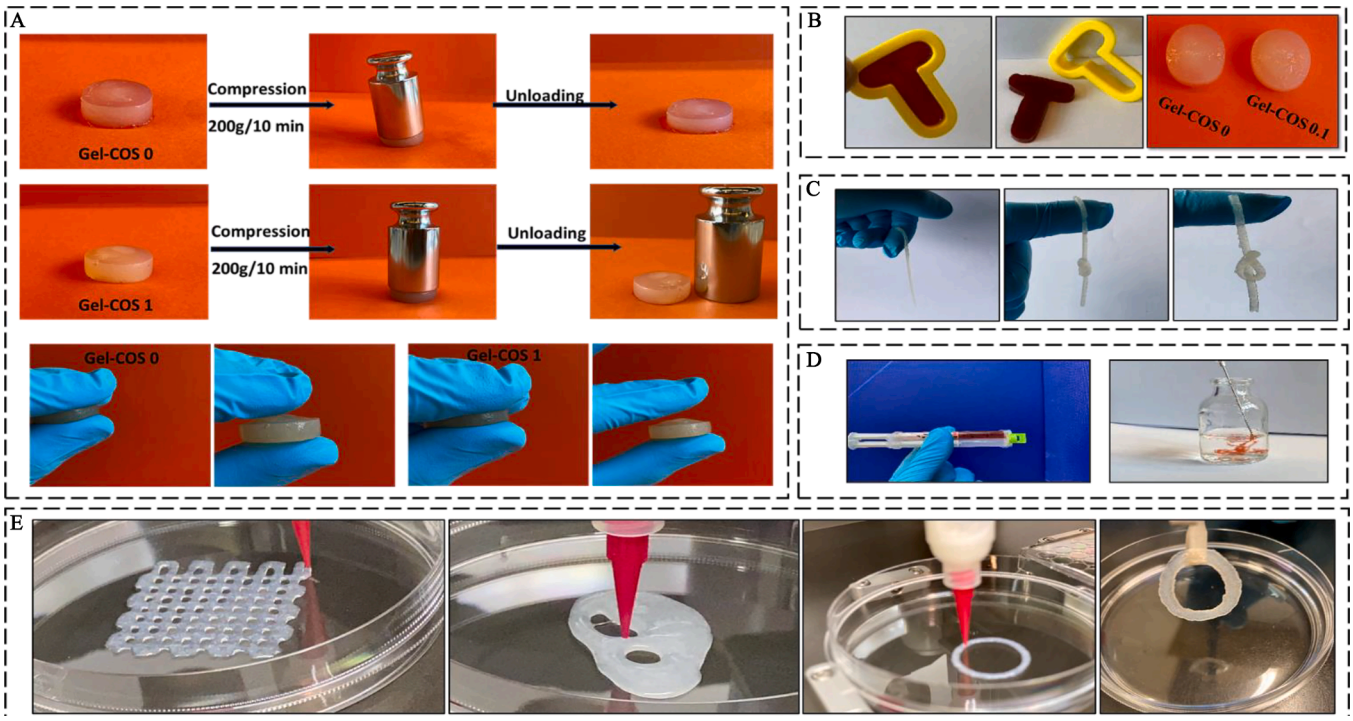

Fig. 4. Mechanical properties and 3D printing ability of Gel-COS hydrogels. (A) Deformation resilience investigation of Gel-COS hydrogels by manual compression test using 200 g weight for 10 min; (B) (f) Moldability of Gel-COS hydrogels using different molds; (C) Foldability and flexibility of GEL-COS hydrogels; (D) Injectability of Gel-COS hydrogels using a double syringe with a 52 G needle; (E). Different types of the object were printed using PHEC (3%) containing HRP and GOx, and co-enzymatic crosslinking was triggered by immersing the objects in a 5.5 mM glucose solution.

3.3. *Physiochemical properties of the hydrogels*

The physicochemical properties of Gel-COS hydrogels were investigated to monitor the effect of COS on the hydrogel properties. The equilibrium swelling ratio (ESR) test (Fig. 2E) exhibited that both hydrogels showed a swelling behavior via immersing in PBS (0.01 M, pH=7.4, 37 °C) solution after 36 h. Indeed, the hydrogels started to swell after two h, and the swelling ratio reached an equilibrium state after 36 h. The Gel-COS 0 exhibited a higher ESR (48.8 ± 2.7 %) compared to the Gel-COS 1 (43.4 ± 1.5 %), indicating the effect of COS on decreasing the swelling ratio of the hydrogel possibly due to intensification of the electrostatic interaction resulting in higher crosslinking density [47]. Moreover, it has been reported that less than 100 % swelling ratio is favorable for wound healing applications due to the limitation of highly swollen hydrogels such as blocking the blood system and pressure on nerve systems [48,49].

Furthermore, the degradation behavior of the Gel-COS hydrogels in lysozyme solution was investigated by the gravimetric method (Fig. 2F). Both Gel-COS hydrogels started the degradation after the first day and continuously degraded for up to 9 days. The hydrogels preserved their shape for up to 6 days, whereas after that, the hydrogels broke into smaller parts, and the degradation continued at a higher rate. The weight loss of both Gel-COS hydrogels was around 95% after 9 days indicating the significant biodegradation of Gel-COS hydrogels in lysozyme solution, which is present in the extracellular matrix of human cartilage. The lysozyme degradation process (enzymatic hydrolysis) is believed to occur at β-1,4 linkages between N-acetyl-glucosamine and glucosamine units of chitosan[21,50]. The hydrogels could preserve their stability at the early stage of the wound healing process, and subsequently, the hydrogel can degrade due to the presence of lysozyme (1 mg/mL) in the extracellular matrix [21].

The microstructure investigation of Gel-COS hydrogels (Fig. 2G) revealed that both Gel-COS 0, and Gel-COS 1, exhibited a porous microstructure with a hierarchical morphology including large pores and randomly distributed microfibrous morphology due to the PHEC formation, which may lead to the generation of *in situ* microfibers prior the co-enzyme mediated crosslinking [25]. Hydrogels' porous structure provides sufficient space required for cell growth and nutrition, and metabolite transportation resulting in proliferation and cell viability [28].

3.4. *Viscoelastic and self-healing properties*

Before evaluating the viscoelastic properties of the hydrogels, we investigated the viscosity of the hydrogel precursors to determine the effect of COS on the electrostatic interaction (Fig. 3A). The addition of COS (1 mg/mL) increased the viscosity of the gel precursor from 6662 to 10,567 mPa.s at a shear rate of 0.1 (1/s). Moreover, by increasing the shear rate, the viscosity of the hydrogel precursors decreased, indicating the Gel-COS precursor's shear-thinning behavior because of dynamic non-covalent interaction suitable for the 3D printability of hydrogels [51,52].

The gelation kinetics were determined via evaluating the storage modulus (G') and loss modulus (G") of hydrogels *versus* time (Fig. 3B). In both hydrogels, the G' is higher than the G'' at 0 time due to the instant PHEC formation, which resulted in non-covalent interactions, leading to an increase in G' [25,53,54]. However, the G' started to further increase by the enzymatic crosslinking to form a C-C or C-O bond as a stable crosslink [55]. Interestingly, the addition of COS to the hydrogel increased the G' from 1049 to 1584 Pa after 10 min due to the increasing electrostatic interaction in the hydrogel.

Similarly, Lv et al. reported that incorporating COS (1%) into the carboxymethyl chitosan-alginate PEC caused secondary gelation resulting in a 10^4 fold higher G' (1 MPa) than the hydrogel without COS (150 Pa) [26]. Furthermore, an amplitude sweep test was carried out to evaluate the viscoelastic features of the hydrogels (Fig 3C). Generally, at the point that G' and G" cross each other, a critical strain indicates the deformation resistance of the materials [33,56]. Indeed, after this point,

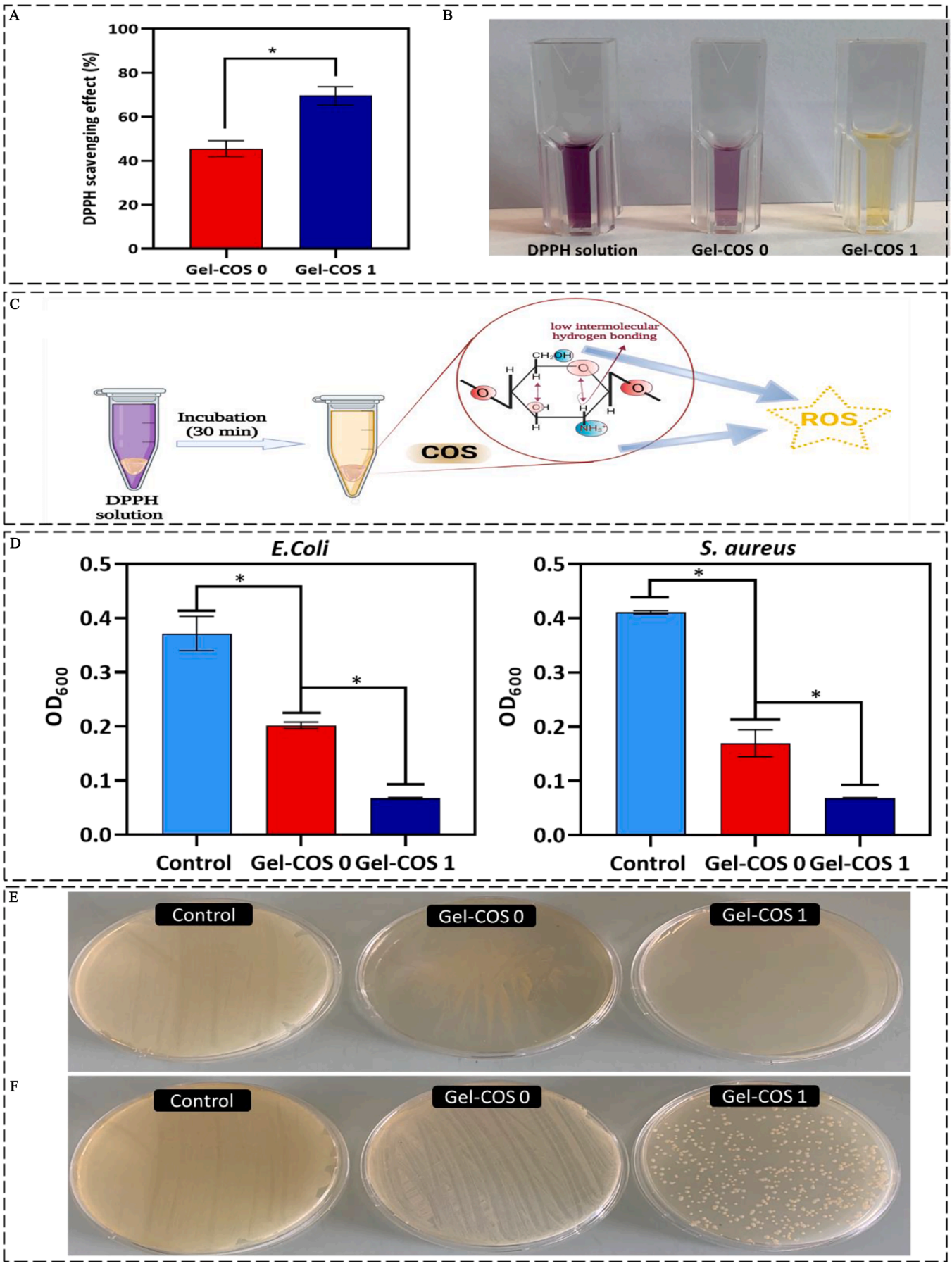

(caption on next page)

Fig. 5. Antioxidant and antibacterial activity of Gel-COS hydrogels. (A) DPPH scavenging activity of Gel-COS 0, and Gel-COS 1; results are shown as % of the DPPH scavenging effect and are the mean ± SD (n = 3, paired measurements). Data were analyzed using one-way ANOVA followed by a Tukey post hoc analysis, *p < 0.05; (B) Images of DPPH reagent's reaction with Gel-COS 0 and Gel-COS 1 after 60 min of incubation, and the color of the DPPH solution transition from dark purple to yellow, showing the DPPH scavenging activity of Gel-COS 1; (C) ROS scavenging activity mechanism of Gel-COS hydrogel due to the scavenging activity of COS with shorter saccharides chains compared to high molecular chitosan, which results in breakage of intermolecular hydrogen bonding, and consequently allow the hydroxyl groups of COS to participate in radical scavenging; (D) Bacterial growth treated by gel-COS 0 and Gel-COS 1 hydrogels after 24 h incubation at 37 °C. Results are shown as optical density (OD) of bacteria suspension and are the mean ± SD (n=3, paired measurements). Data were analyzed using one-way ANOVA followed by a Tukey post hoc analysis, *p < 0.05; (E, F) colony counting assays of the hydrogels against E. coli (E), and *S. aureus* (F).

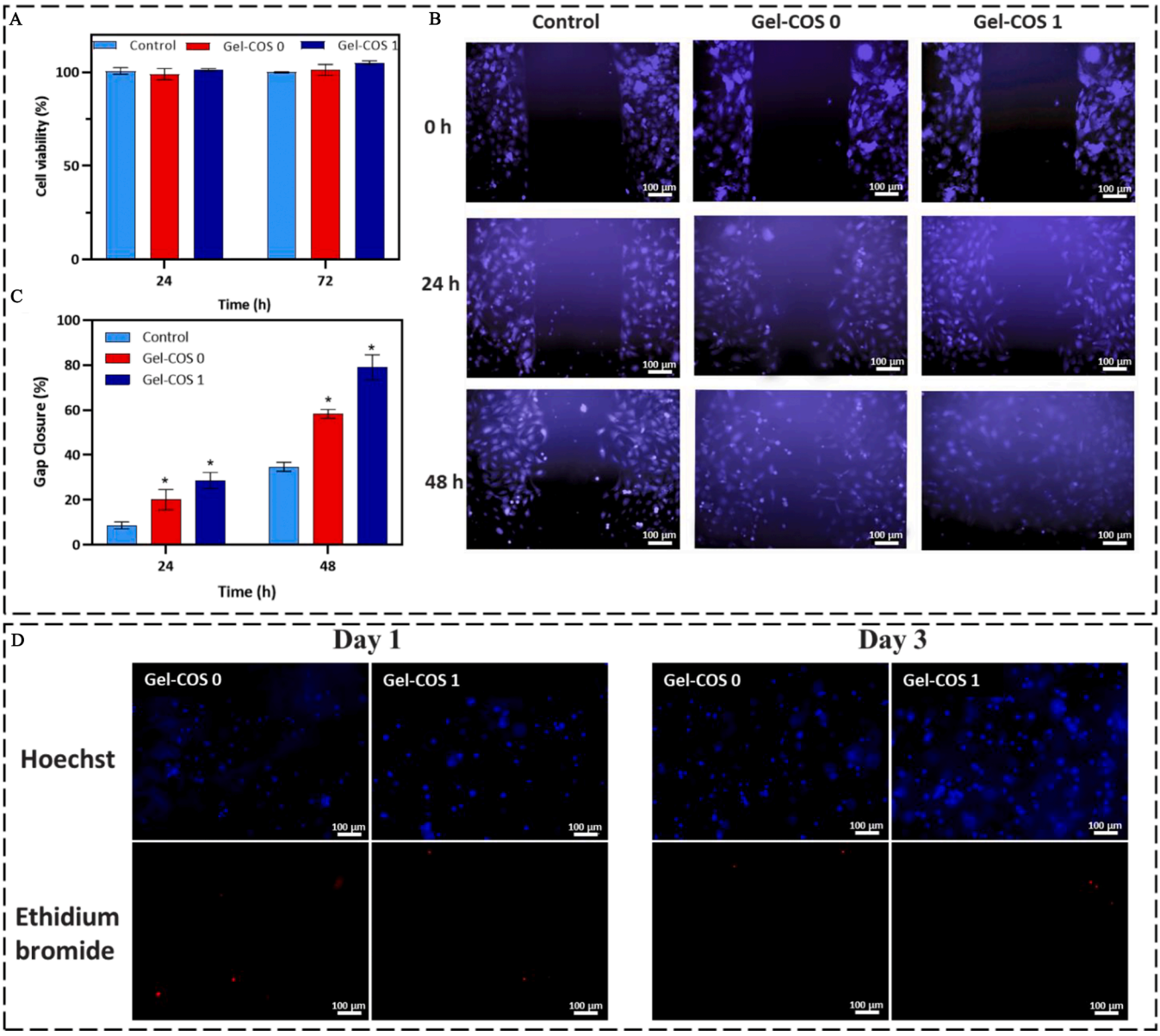

Fig. 6. (A) Cell viability of 3T3-L1 cells seeded on the Gel-COS hydrogel with 0 and 1 mg/mL COS in comparison with a control (cell culture media) after 24 and 72 h. Results are expressed as % of cell viability and are the mean ± SD (n=3; paired measurements); (B) Representative images of *in vitro* 3T3-L1 fibroblast cells undergoing migration treated with control (cell culture media), Gel-COS 0, and Gel-COS 1 hydrogels; (C) Relative gap closure of the cell-free area of 3T3-L1 fibroblast cells. Results are expressed as % gap closure and are the mean ± SD (n = 3; paired measurements). Data were analyzed using a one-way ANOVA test followed by a Tukey post-hoc analysis. *p < 0.05 as compared to the control; (D) Fluorescent microscopic images of 3T3l fibroblasts cell-laden Gel-COS hydrogels via Hoescht and ethidium homodimer I (EH1) (dead cells) after one and three days.

increasing the strain causes a dramatic decrease in the G' exhibiting the disruption of the three-dimensional network [57,58]. The amplitude results showed a critical strain at 530, and 631 % for Gel-COS 0 and Gel-COS 1; besides, the G' of Gel-COS 0, and Gel-COS 1 at the linear viscoelastic region (LVR) was around 1532 Pa and 3052 Pa, respectively. Hence, similar to the gelation kinetic test, the addition of COS increases the G' and the critical strains, indicating that COS improves the hydrogel's stiffness and stability against deformation. After the COS incorporation, the G" of the hydrogel increased from 154 Pa to 308 Pa, indicating that the electrostatic interaction could significantly increase

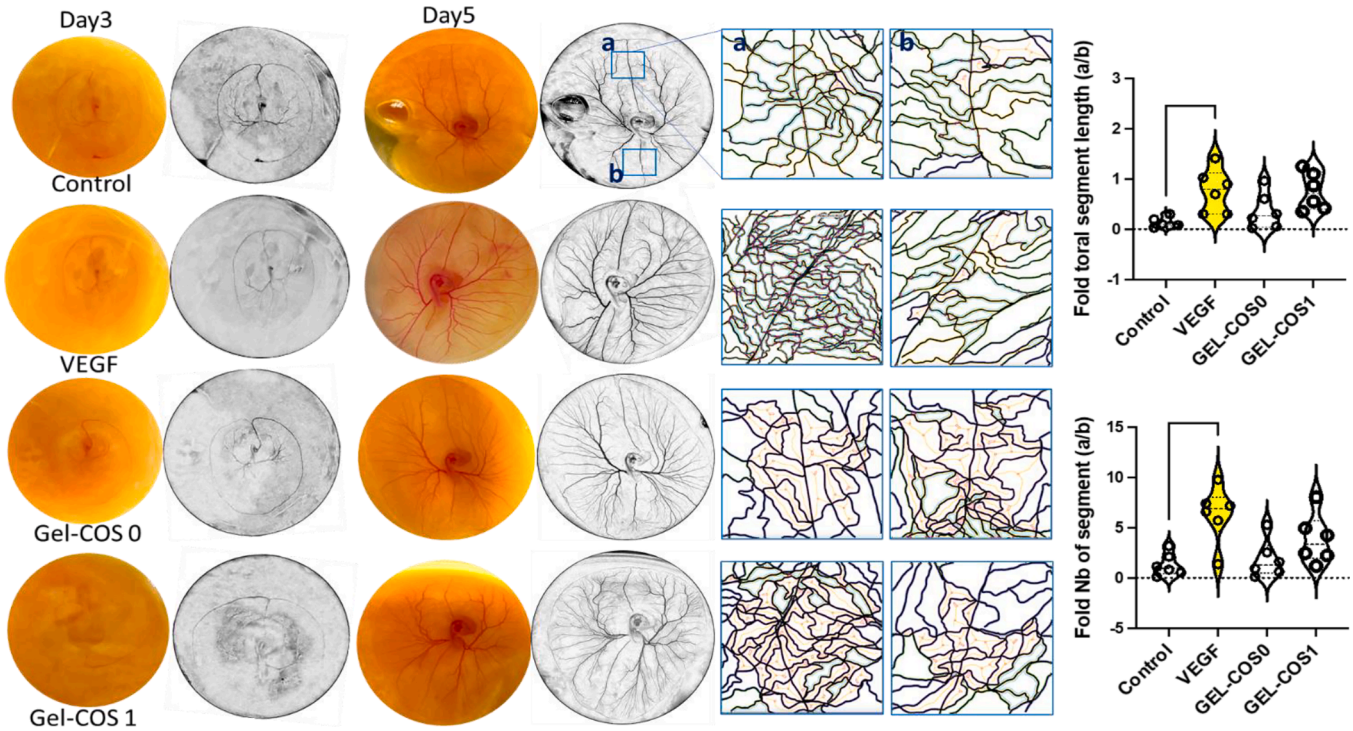

Fig. 7. Evaluation of biocompatibility of the hydrogels in CAM assay. Comparative images (n= 6; paired measurements) were taken from the chick embryo before and after 48 h treatment with Gel-COS 0, Gel-COS 1, and control (no treatment) and vascular endothelial growth factor (VEGF) (positive control). The images were then analyzed using Adobe illustrator and Angiogenesis Analyser in ImageJ. The total segment length and number of segments of the treated part (a) in every embryo are normalized based on other parts of the same embryo (b). 50 ng/mL of VEGF resulted in significant angiogenesis, as indicated by the increase in the total segment length and number of segments. Neither GEL-COS 0 nor GEL-COS 1 caused any toxicity in the treated embryos. GEL-COS 1 resulted in a mild (but not significant) growth in total length and number of vessels. Results are expressed as the mean ± SD. Data were analyzed using a one-way ANOVA, followed by Tukey's posthoc analysis. *$p < 0.05$ vs. Control.

the G" due to the addition of dynamic non-covalent bonding, which increases the hydrogel's physical stability and improves the toughness and viscoelasticity of the gel [59].

Moreover, frequency-dependent changes of G' and G'' in Gel-COS hydrogels were evaluated over the frequency range from 0.1 to 10 Hz (Fig. 3D), and the Gel-COS hydrogels demonstrated a composition-dependent G′ and G″. The incorporation of COS increased the hydrogel's G' from 1273 to 1961 Pa.

For the self-healing capacity of the Gel-COS hydrogel, the two formed hydrogels with and without congo red were combined to see if an intact gel would emerge (Fig. 3E). Two hydrogel pieces started to form a whole hydrogel in an ambient environment without any external interference, thanks to the dynamic non-covalent electrostatic interactions [60]. Furthermore, a rheological assessment of self-healing properties demonstrated that both Gel-COS 0 (Fig. 3F) and Gel-COS 1 (Fig. 3G) could recover the deformation upon a strain of 300% after four cycles. The healing process is due to the association-dissociation process between ionized amine groups of chitosan and COS with the carboxylate groups of sodium alginate as well as weak hydrogen bonds between the polymer chains (Fig. 3G) [23,61]. The results indicate that Gel-COS hydrogels exhibit good self-healing capability, essential for an ideal wound dressing hydrogel. The Gel-COS 0 hydrogel could rebuild some of the broken bonds by comparing the initial G' (2063 Pa) and final G' (920 Pa) after four cycles; besides, the ascending trend of G' during the relaxation cycles (1% strain) confirmed that the broken bond recovery could not occur instantly and also showing that the hydrogels probably need more time to recover more broken bonds.

Interestingly, the broken bonds of the Gel-COS 1 hydrogels recovered faster than Gel-COS 0 considering the higher ascending slope of G' during the relaxation cycles (1% strain). The Gel-COS 1 could recover the initial G' (2165 Pa) to 1145 Pa after four cycles showing that the hydrogel could recover some of the broken bonds. Indeed, the Gel-COS hydrogels could maintain the structure from the nonrecoverable damages via its covalent network. At the same time, non-covalent electrostatic interaction can act as sacrificial bonds, improving the energy dissipation and self-healing ability of hydrogels [62-64].

3.5. Mechanical properties and 3D printing

The deformation and toughness of Gel-COS hydrogels were evaluated by a manual compression test using a 200 g weight and checking the deformation of the hydrogel after 10 min (Fig. 4A). Both hydrogels could preserve their initial structure after the deformation and recover their initial thickness, showing Gel-COS hydrogels' toughness. The flexibility of the hydrogels was shown by pressing with fingers to half of the initial thickness and a fast recovery after the deformation. Indeed, the presence of a high density of electrostatic interactions as a weak and flexible bonding within the polymeric chains of the hydrogel can provide the hydrogel with high toughness and flexibility alongside physical stability due to the phenol-phenol crosslinking as a rigid and brittle covalent bond [65,66]. The hydrogels showed moldability using different shaped molds (T shaped and circular molds) (Fig. 4B) with easy removal from the molds as well as good flexibility by knotting the hydrogels without any fractures (Fig. 4C).

Furthermore, the injectability of the Gel-COS hydrogels was evaluated using a double syringe (L-System, Sulzer, Rotkreuz, Switzerland) (Fig. 2 D). The hydrogel could easily be injected via 52 G needles as a fluid into a PBS buffer and maintain its gel state after injecting, showing the injectability of Gel-COS hydrogels due to the presence of dynamic electrostatic interaction essential for hydrogels for soft tissue repair, particularly for irregularly shaped wounds regeneration [67].

We investigated the 3D printability of Gel-COS hydrogel to

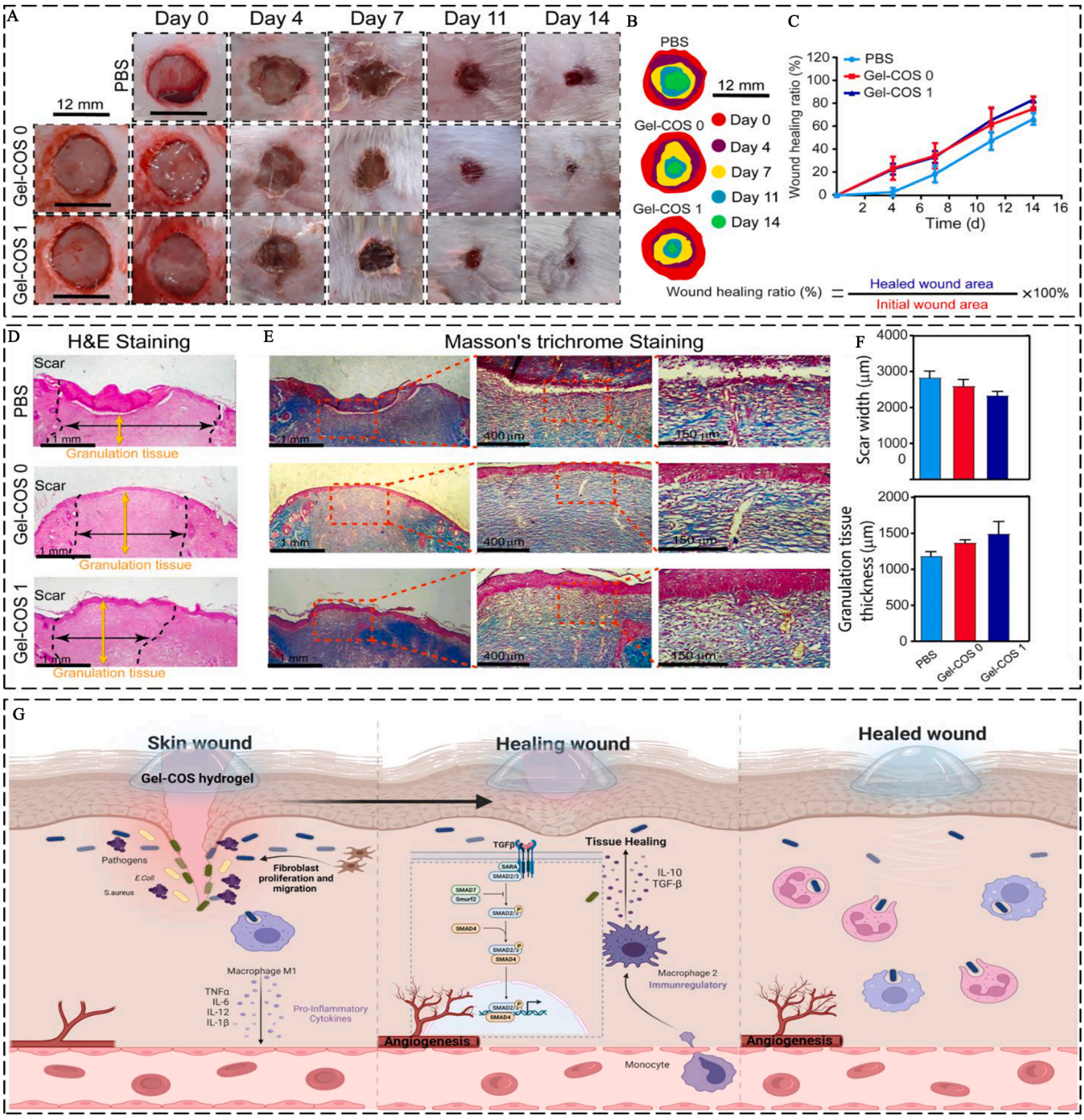

Fig. 8. *In vivo* wound healing performance of different treatment materials, including PBS solution (control group), Gel-COS 0, and Gel-COS 1 hydrogel in a full-thickness skin defect model. (A) Hydrogels (100 μl) or PBS were applied to a 12 mm full-thickness skin wound immediately after wounding. Representative macroscopic images of full-thickness skin wound healing *in vivo* in the control-treated group (PBS), the Gel-COS 0, and Gel-COS 1-treated group at 0, 4, 7, 11, and 14 days after injury; (B) Schematic presentation for the wound healing site on the 4, 7, 11 and 14 days after injury; (C) Quantitation of the rate of wound healing ratio of full-thickness skin wounds were determined by analyzing the wound healed in photos; (D) H&E staining images of wound site tissues from different groups. Neodermis regeneration outline was marked by black dashed, the scar's width was shown by black double-headed arrows. The yellow double-headed arrows demonstrated the thickness of granulation tissue; (E) Masson's trichrome staining of the granulation tissue in control, Gel-COS 0, and Gel-COS 1-treated group on the 14 days of wound healing indicating newly-formed collagen fibers distributed into the granulation tissue; (F) Quantitation of the scar width (black double-headed arrows in d) and granulation tissue thickness (yellow double-headed arrows in d) of different groups after 14 days of injury. Rats, n = 5. Statistical significance was analyzed by one-way ANOVA followed by a Tukey post hoc analysis between multiple groups, and statistical significance was considered as $^{*}p < 0.05$. Data are shown as the mean ± standard deviation; (G) The wound healing mechanism of gel-COS hydrogels, based on superior biological activities of COS such as antioxidant, antibacterial, and anti-inflammatory activities, paves the way for removing ROS, preventing peroxidation damage, and bacterial infection at the early stage of wound healing. Moreover, COS might promote tissue by increasing the proliferation and migration of fibroblast and keratinocytes cells. Besides, COS might induce macrophage transition by reducing the level of inflammatory cytokines, resulting in wound healing acceleration.

determine the possibility of developing a customized hydrogel. We previously showed that the PHEC with a higher than 2 wt% could be printed due to its viscosity and gel-like behavior driven by physically crosslinked phenolated polyelectrolyte complex (PHEC) between phenolated chitosan and alginate [25]. Here, we tested the hydrogel 3D printability using glucose-triggered co-enzymatical crosslinking. The PHEC (3% Ch-Ph, and Alg-Ty) containing COS (1 mg/mL), HRP (1 U/mL) and GOx (10 U/mL) was used as the printing biomaterial ink. The printing process was conducted via a bioplotter pneumatic dispensing system (BioScaffolder 3.2, GeSiM, Germany) at 140 kPa and a speed of 11 $mm.s^{-1}$ using an 25 G plastic needle. The hydrogel ink could be easily injected through the printer nozzle. After printing, the printed objects were exposed to glucose solution (5.5 mM) to induce the co-enzymatically crosslinking through reacting with Gox and gradual generation of H_2O_2, which led to activation of HRP and subsequently phenol-phenol crosslinking [15]. Various examples of 3D-printed hydrogels are shown in Fig. 4E. The co-enzymatically crosslinked printing method can be a promising alternative to conventionally enzymatically crosslinking by HRP, and H_2O_2, particularly for 3D printing applications.

3.6. Antioxidant and antibacterial activity of Gel-COS hydrogels

Antioxidant and antibacterial activities are crucial factors in accelerating the wound healing process[68]. A significant benefit of the hydrogels' antioxidant activity is their ability to suppress oxidative stress in cells and the body [69]. The antioxidant activity of Gel-COS hydrogels was investigated via a DPPH scavenging assay (Fig. 4). The DPPH activity of Gel-COS hydrogel increased from 45.4 ± 2.8 to 69.5 ± 3.3 with the addition of COS to the hydrogel (Fig. 5A). Fig. 5B shows the color change of the DPPH solution reacted with Gel-COS hydrogels. The color changes from a dark purple (DPPH solution) to light purple (Gel-COS 0), and yellow (Gel-COS 1), indicating the decolorization of stable DPPH radicals due to the antioxidant activity of Gel-COS hydrogels. The results revealed that adding COS could significantly increase hydrogel's DPPH scavenging activity due to its advanced antioxidant features derived from its low molecular weight. Indeed, the intermolecular hydrogen bonding is significantly decreased in the COS structure compared to chitosan because of its low molecular weight (< 3 kDa) [70]. Hence, hydroxyl groups (C6) and the amino groups (C2) of COS can easily participate in the reaction with the hydroxyl and superoxide anion radicals, leading to the stable macromolecule radical formation (Fig. 5C) [7,71]. Several studies reported that COS incorporation into hydrogel or scaffolds increased antioxidant activity [72-74].

In addition to the antioxidant, antibacterial properties of a wound dressing hydrogel are also important for wound healing application [75]. Bacterial growth and colony counting assays were carried out to investigate the antibacterial activity of Gel-COS hydrogels against *E. coli* and *S. aureus* as the primary bacteria present in the infected wounds [35]. Both hydrogels inhibit the growth of *E. coli* and *S. aureus* compared to the control (Fig. 5D). The OD_{600} of bacterial suspensions treated by Gel-COS 1 was significantly lower (0.067 ± 0.01 for *E. coli*, 0.068 ± 0.01 for *S. aureus*) compared to the control group (0.37 ± 0.02 for *E. coli* and 0.414 ± 0.02 for *S. aureus*). Hence, the addition of COS led to significant improvement in the bacterial inhibition growth of hydrogel due to the antibacterial activity of COS [76].

Moreover, the colony counting assay exhibited that the colony formation decreased in the Gel-COS 0 and Gel-COS 1 against both tested bacteria compared to the control after 24 h incubation (Figs 5E, F). Both hydrogels showed a higher antibacterial effect against *E. coli* owing to the residual positively charged amino groups on the backbone of chitosan and COS, which could form an impermeable coating on the cell wall of gram-negative bacteria leading to suppressing the metabolic activity [7]. Indeed, no colony formation was observed from the *E. coli* treated by Gel-COS 1 (Fig 5E), while, in the case of *S. aureus* (Fig 5F), colony numbers are higher than the *E.coli* although it decreased significantly compared to the control and Gel-COS 0 groups. Hence, our results showed that Gel-COS 1 possess antibacterial properties, particularly against gram-negative bacteria.

3.7. Cell viability and migration

Proliferation and migration of fibroblasts are critical parameters in the acceleration of the wound healing process induced by the up-regulation of various growth factors such as keratinocyte growth factor (KGF), epidermal growth factor (EGF), and fibronectin resulting in the migration of keratinocyte, and fibroblast and therefore wound healing acceleration [29,77]. The effect of Gel-COS hydrogels on the viability of 3T3-L1 fibroblasts was studied after 24 and 72 h of culture (Fig. 6A). Both Gel-COS 0 and Gel-COS 1 exhibited no significant adverse effect on the cell viability compared to the control. It showed that the dual crosslinking system was compatible without any adverse effects on the cell viability.

The effect of Gel-COS hydrogels on the migration of 3T3-L1 fibroblasts was investigated using *in vitro* wound healing assay (Fig. 6B). 3T3-L1 fibroblasts treated with both Gel-COS 0 and Gel-COS 1 showed a significantly higher migration, witnessed by gap closure, after 24 and 48 h compared to the control group. Indeed, after 24 h, the gap closures for the control, Gel-COS 0, and Gel-COS 1 were 8.3±1.2, 20.1±3.7, and 28.6 ±2.8%, respectively (Fig. 6C). Besides, after 48 h, the cells treated with the hydrogels showed a higher tendency to cover the gap, with 58.3±1.2 and 79.1±4.5% of gap closure for Gel-COS 0 and Gel-COS 1, respectively, compared to the control (34.7±1.6%). These data corroborated those from recent studies reporting that COS increased the migration of fibroblasts and human umbilical vein endothelial cells (HUVECs) [27, 78].

To further evaluate the cell encapsulation capability of Gel-COS hydrogels for cell therapy and wound healing applications, 3T3-L1 fibroblast cells were incorporated into Gel-COS hydrogels to form a cell-laden hydrogel, and the cell nuclei distribution, as well as cell viability, were assessed (Fig. 6D). The 3T3-L1 fibroblast cells showed a uniform cell spreading distribution within the hydrogels after 1 and 3 days of culture, indicating the Gel-COS hydrogel ability for homogenous cell spreading. Both Gel-COS hydrogels exhibited a low number of dead cells (stained red with ethidium homodimer I), indicating Gel-COS cytocompatibility. The results agree with previous studies reporting the promotion of cell adhesion, and migration capability of COS-containing biomaterials [72,79]. Hence, our results revealed that co-enzymatically mediated crosslinking is a compatible method for cell encapsulation due to the mild reaction and gradual release of H_2O_2 via the GOx reaction. Kim et al. reported a high cytocompatibility by using a co-enzymatically crosslinking based on GOx and HRP compared to H_2O_2 and HRP crosslinking systems [15]. Another recent study reported a higher cytocompatibility of a 3D printed hydrogel-based using GOx/HRP than directly supplying H_2O_2 [45].

3.8. Angiogenesis activity

An ideal wound dressing material must be integrated with the existing host tissue through an active blood vessel network [80]. CAM assay is a standard method to assess the biocompatibility of newly developed biomaterials [40]. Hence, we evaluated the response of CAMs to Gel-COS 0 and Gel-COS 1 on the total length and number of junctions of the formed vessel using an angiogenesis analyzer in ImageJ (Fig. 7). The methods were validated by vascular endothelial growth factor (VEGF) as the positive control. VEGF significantly increases both the number and length of the new blood vessels ($p < 0.05$). Although Gel-COS 1 resulted in a mild growth in the density and length of blood vessels, the difference between control and Gel-COS 1 was not statistically significant. The results show that both Gel-COS 0 and Gel-COS 1 did not have any cytotoxic effect on the blood vessel formation within 48 h of incubation. Angiogenic properties of an optimal concentration of

COS (4 μg/mL) and polymerization degree of 5 have been shown previously [81]. In addition, COS effectively can enhance tissue regeneration and angiogenesis by inducing the synthesis of angiogenic factors such as EGF,[2] VEGF-D,[3] and basic fibroblast growth factor (bFGF) [7].

3.9. Wound healing in a full-thickness skin defect model

The wound healing potential of Gel-COS hydrogels were investigated in a full-thickness skin defect model. For this purpose, a circular wound (12 mm full-thickness) was made on the rat skin and subsequently treated with different materials, including PBS solution (control group), 100 μl of Gel-COS 0, and Gel-COS 1 hydrogel. All the rats survived well without infection in the full-thickness wounds. As shown in Fig. 8A, Gel-COS 0, and Gel-COS 1 -treated groups showed significantly enhanced wound healing at day 14 post-injury of treatment in comparison with the control-treated group, in which wound healing ratios were 75.7 ± 9.2 and 83.6 ± 2.1 for Gel-COS 0, and Gel-COS 1 -treated *vs.* 66.8 ± 4.7% for the control-treated group (Fig. 8C). Hence, an enhancement of the wound healing ratio by hydrogels was recorded compared to the control-treated group on day 14 post-injury (Fig. 8B). The current study results indicated that control-treated group treatment was not able to promote wound healing.

To further investigate wound healing, wound sites were stained with hematoxylin and eosin (H&E) to monitor regenerated skin tissues. Although no significant difference was observed in skin photos between the Gel-COS 0 and Gel-COS 1-treated group at any time, H&E staining (Fig. 8D) revealed that the Gel-COS 1 -treated group enhanced epithelialization and granulation at 14 days compared with the Gel-COS 0 and control-treated group. The wounds treated with Gel-COS 0 and Gel-COS 1 showed less scar tissue developed (black double-headed arrow) than the control-treated group ($p < 0.05$) (Fig. 8F). In addition, quantification of the granulation tissue (GT) thickness revealed that total thickness growth in the Gel-COS 0 and Gel-COS 1-treated groups was 1.24 ± 0.09 and 1.28 ± 0.15-fold higher, respectively, compared to the control-treated group (Fig. 8F). Furthermore, quantification of the scar width demonstrated that the Gel-COS 0 and Gel-COS 1-treated groups had a 2630 ± 366 and 2370 ± 237 μm, which is lower width than the control-treated group (2880 ± 338 μm) (Fig. 8F). The Gel-COS 0 and Gel-COS 1-treated wounds showed better re-epithelialization, evidenced by the more minor residual epithelial defects than PBS-treated wounds after 7 and 14 days of treatment (Supplementary Fig. 1 and Fig. 1e).

The abundance of collagen reflects the quality of the regenerated skin tissue. Therefore, to confirm the efficacy of Gel-COS hydrogels in skin wound regeneration, sections of wound tissue on day 14 were stained using Masson's trichrome, in which collagen and nucleus were stained in blue and dark blue, respectively (Figs. S1 and 8E). The Gel-COS 0 and Gel-COS 1 hydrogels exhibited an integration with the dermis; in both hydrogel groups, collagen bundles were regenerated in a regular arrangement and extensively distributed, while the control-treated group exhibited a loosely packed collagen fibers with an irregular arrangement. Furthermore, the defect site for the control-treated group is completely recognizable after 7 and 14 days of post-injury (Figs. S1 and 8E).

The results of our study indicated that the Gel-COS 1 hydrogel exhibited the best performance compared to the control and Gel-COS 0 hydrogel in wound healing. We proposed a model of the wound healing mechanism of gel-COS hydrogels in which the superior biological activity of COS, such as antioxidant, antibacterial, and anti-inflammatory activities, may effectively remove ROS and prevent peroxidation damage at the wound site and could effectively prevent bacterial infection at the wound site compared to high molecular chitosan [82-84]. Besides, COS may promote the proliferation and migration of fibroblasts; furthermore, COS may promote wound healing by miR-27 up-regulating and activating the transforming growth factor-beta (TGF-β)-1-Smad2/3 pathway[85]. The anti-inflammatory activity of COS may also leads to the efficient macrophage transition (M1 to M2) via preventing the generation of pro-inflammatory cytokines (Fig. 8G) therefore may contribute to epithelial tissue formation in wound healing [7,84,85] (Fig. 8G).

4. Conclusion

In this study, we successfully developed a biocompatible hydrogel (Gel-COS) via a double crosslinking strategy, including co-enzymatically mediated crosslinking via Gox/HRP and phenolated polyelectrolyte complex (PHEC). The crosslinking was initiated with a spontaneous electrostatic interaction between positively charged chitosan and chitooligosaccharides (COS) with negatively charged alginate, followed by a mild co-enzymatic crosslinking triggered by the gradually released H_2O_2 from the GOx reaction. The addition of COS improved the rheological properties of the hydrogel and decreased the swelling ratio due to the intensification of the electrostatic interactions because of the presence of positively charged amino groups on the backbone of the COS, resulting in higher crosslinking density. The hydrogels exhibited moldability, injectability, self-healing, toughness, flexibility, and 3D printability thanks to the synergy of covalent co-enzymatic crosslinking as rigid and brittle bonds as well as electrostatic interaction as weak and flexible bonds. The biological investigation revealed that incorporation of COS significantly increases the DPPH radical scavenging activity of hydrogel and antibacterial activity of hydrogel against both gram-negative and positive bacteria thanks to its enhanced biological activity due to its low molecular weight. Moreover, the Gel-COS hydrogels exhibited good cell viability of 3D encapsulated 3T3-L1 fibroblast; besides, the proliferation and migration of 3T3-L1, as well as positive effect on the angiogenesis activity of hydrogel. The *in vivo* wound healing investigation revealed higher wound closure, granulation tissue, collagen regeneration, and less scar width after 14 days. Hence, the Gel-COS hydrogel holds great potential as a wound dressing hydrogel due to its unique properties such as high toughness, moldability, self-healing, antioxidant, antibacterial, injectability, and serves as a minimally invasive approach to reducing the chance of wound infections and expedite skin regeneration. As such, gel-COS may provide additional therapeutic leverage to treat diabetic foot ulcers and venous leg ulcers that are very disabling for the patients.

Declaration of Competing Interest

The authors declare that they have no known competing financial interests or personal relationships that could have appeared to influence the work reported in this paper.

Acknowledgments

H.J and A.S. acknowledge funding from Innoviris Brussels, Belgium (https://innoviris.brussels) under the project 2019 – BRIDGE – 4: RE4BRU. H.J also acknowledge the FNRS Gustave Boël-Sofina Fellowship. The content is solely the authors' responsibility and does not necessarily represent the official views of the above-mentioned funding agency. The authors acknowledge the facilities and technical assistance from CARAMAT staff at the ULB; besides, the authors acknowledge Dr. Véronique Fontaine for the facilities and scientific assistance for performing the antibacterial test. D.P. acknowledges the support from the Polish National Science Centre (2016/23/D/ST8/01267) and from the Academia Iuvenum, Wrocław University of Science and Technology. The authors acknowledge Dr. Jonathan Goole for the facilities and scientific assistance for performing the zeta potential test.

[2] Epidermal growth factor (EGF)
[3] Vascular endothelial growth factor D (VEGF-D)

Supplementary materials

Supplementary material associated with this article can be found, in the online version, at doi:10.1016/j.apmt.2022.101581.

References

[1] S. Das, A.B. Baker, Front. Bioeng. Biotech. 4 (2016) 82.
[2] T.T.H. Thi, et al., Macromol. Res. 27 (8) (2019) 811.
[3] A. Gaspar-Pintiliescu, et al., Int. J. Biol. Macromol. 138 (2019) 854.
[4] S. Özbilgin, et al., J. Ethnopharmacol. 224 (2018) 400.
[5] L. Yarmolinsky, et al., Plants 8 (12) (2019) 609.
[6] J. Koehler, et al., Eur. Polym. J. 100 (2018) 1.
[7] H. Jafari, et al., Mater. Sci. Eng. C (2020), 111266.
[8] C. Muanprasat, V. Chatsudthipong, Pharmacol. Ther. 170 (2017) 80.
[9] L. Nie, et al., Mater. Today Commun. (2022), 103697.
[10] S. Sakai, M. Nakahata, Chem. Asian J. 12 (24) (2017) 3098.
[11] Y. Liang, et al., J. Colloid Interface Sci. 556 (2019) 514.
[12] S. Liu, et al., ACS Appl. Mater. Interfaces 12 (25) (2020) 27876.
[13] O. Hasturk, et al., Biomaterials 232 (2020), 119720.
[14] N.R. Raia, et al., Biomaterials 233 (2020), 119729.
[15] B.Y. Kim, et al., Macromol. Biosci. 16 (11) (2016) 1570.
[16] M. Yao, et al., Biomater. Sci. 7 (10) (2019) 4088.
[17] T. Sahana, P. Rekha, Mol. Biol. Rep. 45 (6) (2018) 2857.
[18] L. Cai, et al., Acta Biomater. 113 (2020) 84.
[19] A. Moeini, et al., Carbohydr. Polym. 233 (2020), 115839.
[20] N.T. Phuong, et al., J. Bioact. Compat. Polym. 30 (4) (2015) 412.
[21] R. Jin, et al., Polym. Chem. 5 (2) (2014) 391.
[22] S.V. Gohil, et al., J. Mater. Chem. B 3 (27) (2015) 5511.
[23] N. Barroso, et al., Eur. Polym. J. 120 (2019), 109268.
[24] S. Potiwiput, et al., Mater. Chem. Phys. 241 (2020), 122354.
[25] H. Jafari, et al., Green Chem. (2022).
[26] X. Lv, et al., Carbohydr. Polym. 205 (2019) 312.
[27] H. Jafari, et al., Chem. Eng. J. Adv. 7 (2021), 100113.
[28] P. Le Thi, et al., Acta Biomater. 103 (2020) 142.
[29] D.L. Tran, et al., Progress Natr. Sci. Mater. Int. 30 (5) (2020) 661.
[30] F. Chen, et al., Sci. Rep. 6 (1) (2016) 1.
[31] H. Jafari, et al., ACS Biomater. Sci. Eng. 4 (7) (2018) 2484.
[32] G.K. Wasupalli, D. Verma, Int. J. Biol. Macromol. 114 (2018) 10.
[33] J. Liu, et al., Carbohydr. Polym. 227 (2020), 115335.
[34] H.C. Kim, et al., Mater. Lett. (2021), 129987.
[35] G. Tao, et al., Mater. Sci. Eng. C 119 (2021), 111597.
[36] P. Le Thi, et al., Mater. Sci. Eng. C 92 (2018) 52.
[37] H. Xu, et al., J. Biomed. Mater. Res. Part A (2021).
[38] M. Parekh, et al., Acta Ophthalmol. (Copenh) 96 (6) (2018) e718.
[39] A.A. Zahid, et al., Int. J. Biol. Macromol. 136 (2019) 901.
[40] N.i. Mangir, et al., ACS Biomater. Sci. Eng. 5 (7) (2019) 3190.
[41] B. Bi, et al., Colloids Surf. B 175 (2019) 614.
[42] M. Kurisawa, et al., Chem. Commun. (34) (2005) 4312.
[43] S.M. Davachi, et al., Mater. Today Commun. 30 (2022), 103230.
[44] S. Saghati, et al., J. Biomater. Appl. 36 (5) (2021) 789.
[45] K. Peng, et al., ACS Appl. Bio Mater. (2021).
[46] D. Komoto, et al., Int. J. Biol. Macromol. 126 (2019) 54.
[47] G. Kopplin, et al., RSC Adv. 11 (23) (2021) 13780.
[48] T.T. Hoang Thi, et al., Biopolymers 109 (1) (2018) e23077.
[49] P. Le Thi, et al., J. Mater. Chem. B 5 (4) (2017) 757.
[50] R. Jin, et al., Biomaterials 30 (13) (2009) 2544.
[51] S. Uman, et al., J. Appl. Polym. Sci. 137 (25) (2020) 48668.
[52] M. Truong, L. Walker, Langmuir 18 (6) (2002) 2024.
[53] H.V. Sæther, et al., Carbohydr. Polym. 74 (4) (2008) 813.
[54] S.J. Florczyk, et al., J. Biomed. Mater. Res. Part A 98 (4) (2011) 614.
[55] M. Khanmohammadi, et al., Biomater. Sci. 6 (6) (2018) 1286.
[56] A.H. Clark, Structural and Mechanical Properties of Biopolymer gels. In Food polymers, Gels and Colloids, Elsevier, 1991, p. 322.
[57] J.R. Silverman, et al., ACS Appl. Mater. Interfaces 9 (49) (2017) 43197.
[58] H. Jafari, et al., Polym. Compos. 41 (2) (2020) 624.
[59] J. Cao, et al., Adv. Funct. Mater. 28 (23) (2018), 1800739.
[60] J. Zhang, et al., Mater. Sci. Eng. C 117 (2020), 111298.
[61] S. Maiz-Fernández, et al., Polymers 12 (10) (2020) 2261.
[62] F. Chen, et al., Polymer 168 (2019) 159.
[63] C. Cui, et al., ACS Appl. Mater. Interfaces 11 (42) (2019) 39228.
[64] L. Wang, et al., ACS Appl. Mater. Interfaces 11 (3) (2018) 3506.
[65] J. Cao, et al., Carbohydr. Polym. 242 (2020), 116420.
[66] D. Gan, et al., Adv. Funct. Mater. 29 (1) (2019), 1805964.
[67] C.B. Rodell, et al., Adv. Mater. 28 (38) (2016) 8419.
[68] S. Sellimi, et al., Int. J. Biol. Macromol. 119 (2018) 633.
[69] S. Zhang, et al., Chem. Eng. J. 392 (2020), 123775.
[70] S.A. Ismail, Biocatal. Agric. Biotechnol. 20 (2019), 101269.
[71] R. Cao, et al., J. Sci. Food Agric. 98 (6) (2018) 2422.
[72] H.-H. Park, et al., Carbohydr. Polym. 198 (2018) 197.
[73] A. Singh, et al., Int. J. Food Sci. Tech. 54 (10) (2019) 2831.
[74] G.-W. Oh, et al., Carbohydr. Polym. 252 (2021), 117145.
[75] J. Qu, et al., Biomaterials 183 (2018) 185.
[76] Á. Sánchez, et al., Carbohydr. Polym. 157 (2017) 251.
[77] S. Ellis, et al., Curr. Dermatol. Rep. 7 (4) (2018) 350.
[78] Y. Chen, et al., Mater. Sci. Eng. C 94 (2019) 1020.
[79] P. Chandika, et al., Mater. Sci. Eng. C 121 (2021), 111871.
[80] R. Augustine, et al., J. Mater. Chem. B 5 (24) (2017) 4660.
[81] X. Huang, et al., ACS Biomater. Sci. Eng. 6 (3) (2020) 1614.
[82] W. Hao, et al., Carbohydr. Polym. 252 (2021), 117206.
[83] I. Hamed, et al., Trends Food Sci. Technol. 48 (2016) 40.
[84] R.C.L.C. de Andrade, et al., Int. J. Mol. Sci. 22 (19) (2021) 10631.
[85] Y. Wang, et al., Mol. Neurobiol. 53 (1) (2016) 28.
[86] L. Nie, D. Chen, S.P. Zhong, Q. Shi, Y. Sun, C. Politis, A. Shavandi, Injectable Cell-laden poly(N-isopropylacrylamide)/Chitosan Hydrogel Reinforced via Graphene Oxide and Incorporated with Dual-growth Factors, Mater. Lett. 280 (2020), https://doi.org/10.1016/j.matlet.2020.128572.
[87] Y. Deng, A. Shavandi, O. Okoro, L. Nie, Alginate modification via click chemistry for biomedical applications, Carbohydr. Polym. 270 (2021) 118360, https://doi.org/10.1016/j.carbpol.2021.118360.
[88] H. Jafari, P. Ghaffari-bohlouli, D. Podstawczyk, L. Nie, A. Shavandi, Tannic acid post-treatment of enzymatically crosslinked chitosanalginate hydrogels for biomedical applications, Carbohydr. Polym. (2022), 119844, https://doi.org/10.1016/j.carbpol.2022.119844.